

Metasurface-Enabled Cavity Antenna: Beam Steering With Dramatically Reduced Fed Elements

Kayode Adedotun Oyesina^{ID}, *Student Member, IEEE*, and Alex M. H. Wong^{PD}, *Senior Member, IEEE*

Abstract—We present a metasurface-enabled cavity antenna that achieves full beam steering but features a significantly reduced number of fed elements. To create this antenna, we first excite a traveling wave in a cavity enclosed by an active metasurface, then form the desired radiation by leaking the cavity wave through a perforated top plate. We hence achieve a steerable antenna for which the number of fed elements scales with the perimeter and not the area of the radiation aperture. In this letter, we report two models of this cavity antenna whose beamwidths and sidelobe levels closely resemble a traditional microstrip patch array of the same aperture size. Hence, dramatic savings in feed cost and complexity are achieved without compromising the antenna gain, the beam shape, or steerability. The proposed antennas shall attract strong interest in highly directive millimeter-wave beamforming applications.

Index Terms—Active metasurface, directive antennas, Huygens' sources, leaky-wave antennas, metamaterial, phased arrays.

I. INTRODUCTION

ANTENNAS with low profile and high directivity have become highly desirable for many applications, which for example include communication, imaging, and autonomous vehicular technology. The most common method to achieve directed radiation is to use a phased array antenna, where beam steering is achieved by maintaining a linear phase progression among array elements. To avoid grating lobes, elemental spacing in a phased array antenna should be kept at $d \leq \lambda/2$, hence, the total number of radiating elements in a phased array is dependent on the aperture area. However, the requirement of exciting individual radiating elements at different phases raises the cost of the phased array antenna, especially for large array sizes and for high-frequency operation in the millimeter (mm)-wave regime, because of the high cost associated with the power-dividing and phase-shifting circuitry [1]–[3]. Furthermore, the requirement for a complicated feed network also necessitates a large volume to house the required circuitry, and in some cases, the installation of associated cooling components. Hence, an alternative steerable high-gain antenna with reduced feed network complexity is highly desired.

With advances in metamaterial and metasurfaces, exciting new possibilities emerge [4]–[8]. These artificially engineered

Manuscript received December 31, 2019; accepted February 5, 2020. Date of publication February 12, 2020; date of current version April 17, 2020. This work was supported by an Early Career Scheme from the Research Grants Council of the Hong Kong under Grant 9048152. (Corresponding author: Kayode Adedotun Oyesina.)

The authors are with the State Key Laboratory of Terahertz and Millimeter Waves, Department of Electrical Engineering, City University of Hong Kong, Hong Kong (e-mail: kaoyesina2-c@my.cityu.edu.hk; alex.mh.wong@cityu.edu.hk).

Digital Object Identifier 10.1109/LAWP.2020.2973507

materials have been applied to a myriad of applications, such as cloaking, revolutionary electronics, and antenna enhancement [9]. A brief review of metamaterial-enhanced antennas is given in [10] and [11]. Demonstrated applications include the formation of novel substrates [12], metamaterial lens antennas [13], and leaky-wave antennas [14], [15], among others. Recently, space–time modulated metasurface antennas are proposed, which can steer antenna beam using control biases with simplified feeds [16]. However, the metasurface element spacing remains subwavelength, and steerability is also related to the aperture area, much like the 2-D patch antenna array. This means a complicated signal feed with a multitude of bias lines is needed to achieve beam steering for an electrically large aperture.

In this letter, we propose and demonstrate in simulation two metasurface-enabled cavity antennas that we name the Huygens' box antenna (HBA)—a Huygens' metasurface-based, fully steerable, highly directive antenna for which the number of fed elements scales with the perimeter of the radiating aperture. We design the HBA in the following manner. We first form an enclosure by wrapping an active Huygens' metasurface around a region of interest. We then generate a propagating plane wave in the aforesaid enclosure. Finally, we allow the generated cavity waves to radiate by perforating the aperture on one side of the cavity. After formulating the design process, we will report simulation results for the two HBA designs—TEM and TM1 models, for frequencies of 1 and 60 GHz. While the TEM model encloses a metamaterial, the TM1 model uses an air cavity and thereby mitigates complications and bandwidth restrictions, which may come with the use of a metamaterial. We shall show that in each case, the designed HBAs feature dramatically reduced numbers of elements, but nonetheless achieve beamwidths and sidelobe levels comparable to microstrip patch array antennas of similar aperture sizes.

II. HUYGENS' BOX CONCEPT

We begin by overviewing the Huygens' box concept, which arises from considerations on the equivalence principle and electromagnetic boundary conditions. Wong and Eleftheriades [17], [18] have shown that the active Huygens' source of Fig. 1(a) can be placed in a 2-D parallel-plate environment of Fig. 1(b). Further simplification by adapting the electromagnetic image theory results in the single-filament equivalent of Fig. 1(c). For practical implementation of the current filament, a monopole antenna will suffice as it functions similarly to a current filament in coupling to propagating modes within the parallel-plate environment. Therefore, we enclose a region of space with the perfect electric conductor (PEC)-backed single-filament active Huygens' metasurface elements of Fig. 1(c). The distance between the elements is kept at a value less than half-wavelength.

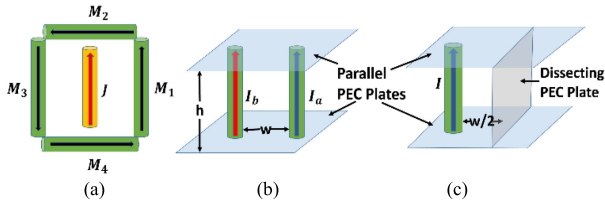


Fig. 1. (a) Simple active Huygens' source. Central current filament constitutes an electric current flow while the magnetic current flows in the outer filament loop. (b) Twin current filament active Huygens' source with copropagating I_a and I_b constituting an effective electric current and counter-propagating I_a and I_b constituting an effective magnetic current. (c) PEC-backed single-filament active Huygens' source equivalent.

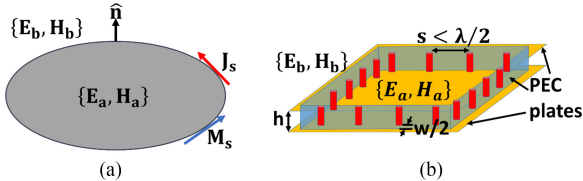


Fig. 2. (a) Electromagnetic equivalence principle, relating a set of surface currents $\{J_s, M_s\}$ to fields on either side of a boundary. (b) Typical Huygens' box developed from the equivalence principle by arranging an array of simplified Huygens' sources.

We call this contraption the Huygens' box [19]–[21]. Fig. 2 depicts the transformation of the equivalence principle into the Huygens' box. We set the desired electromagnetic field within the Huygens' box and set the field outside the enclosure to zero. Then, we invoke electromagnetic equivalence to calculate necessary excitation currents

$$\mathbf{M}_s = -\hat{\mathbf{n}} \times (\mathbf{E}_b - \mathbf{E}_a), \quad \mathbf{J}_s = \hat{\mathbf{n}} \times (\mathbf{H}_b - \mathbf{H}_a). \quad (1)$$

In our previous works, we have applied this method to achieve arbitrary waveform generation in various box sizes and geometries [18]–[21].

III. HUYGENS' BOX ANTENNA

In this letter, we generate traveling plane waves in the Huygens' box cavity, then we develop a highly directive antenna by opening up subwavelength perforations on the top metallic plate of the Huygens' box, thus allowing the cavity wave to radiate. Since the radiated beam emanates from an aperture of electromagnetic fields with uniform amplitude and linear phase progression, the resulting radiation pattern is very much similar to that of a phased array. The radiation direction can be controlled by tuning the cavity wave's travel direction and wavenumber. In the following, we present two HBA designs that generate cavity waves that can be coupled into directive radiation.

A. TEM Huygens' Box Antenna

Fig. 3(a) shows the HBA with a single-layer Huygens' metasurface element enclosing a region of space within a parallel-plate waveguide. We have previously demonstrated the generation of TEM traveling waves, with arbitrary travel direction in the xy plane, in this Huygens' box [17]–[21]. We control the elevation (θ) and azimuthal (ϕ) radiation direction by engineering the cavity material and the cavity wave's travel direction, respectively. For radiation in the elevation direction θ , one needs to match the cavity wave's wavenumber to the radiated

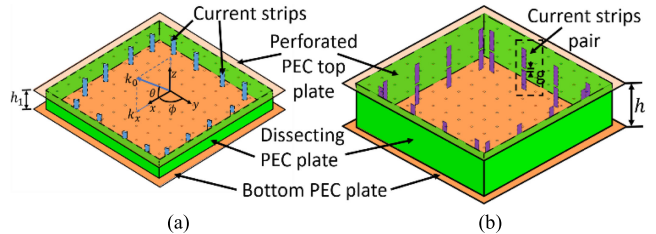


Fig. 3. HBA models. (a) TEM enclosing a metamaterial region with a single layer of Huygens' metasurface elements. (b) TM1 enclosing a region of free space with two layers of Huygens' metasurface elements.

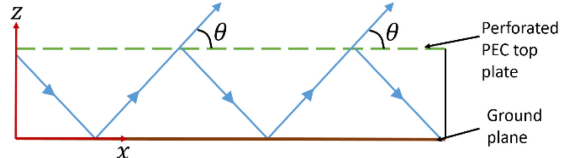


Fig. 4. Ray direction and wavefront direction of a TM1 plane wave between parallel planes.

wave's horizontal spatial frequency

$$k_{\text{cav}} = k_0 n = k_0 \cos \theta \Rightarrow n = \cos \theta. \quad (2)$$

We achieve this by filling the cavity with a dielectric, with $\varepsilon_r = n^2 = \cos^2 \theta$. The required dielectric, with $0 \leq \varepsilon_r \leq 1$, can be readily engineered using metamaterial technology [22], for example using a 2-D array of z -directed metallic wires.

For radiation into the azimuthal direction ϕ , we examine the electromagnetic fields within the cavity, which are given by

$$\begin{aligned} \mathbf{E}(x, y) &= E_0 e^{-j(k_x x + k_y y)} \hat{\mathbf{z}} \\ \mathbf{H}(x, y) &= \frac{\mathbf{E}(x, y)}{\eta} (\sin \phi \hat{\mathbf{x}} - \cos \phi \hat{\mathbf{y}}) \end{aligned} \quad (3)$$

where $k_x = k_0 n \cos \phi$ and $k_y = k_0 n \sin \phi$. Substituting these fields into (1) along the Huygens' box boundary will give us the electric and magnetic currents of the corresponding excitation. For our element of choice, the electric field is shorted by the PEC back plate, and the excitation current along the Huygens' box boundary is related to the magnetic field through [19]

$$I = j (s M_s) / (\omega \mu_0 w) \quad (4)$$

where w and s are as defined in Fig. 2(b). The currents are placed equidistant along the Huygens' box boundary and should function properly as long as their spacing is less than half of the propagation wavelength. Solving (4) at the location of the current elements yields a set of currents, the excitation of which will generate the propagating cavity wave at the desired angle. We have hence achieved control of both elevation and azimuthal radiation directions.

B. TM1 Huygens' Box Antenna

To increase the practicality of the HBA, we further propose an HBA model that uses an air cavity. Fig. 3(b) shows this HBA with two layers of Huygens' metasurface elements along the z -direction, which can be used to excite TM1 traveling waves. Fig. 4 shows a ray diagram depicting the radiation mechanism from the cavity. The height of the air-filled cavity is expanded to $h = \lambda/(2\cos \theta)$ to achieve phase matching between the cavity wave and radiation at the desired elevation angle θ [23]. As

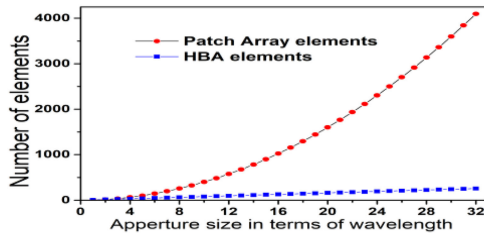


Fig. 5. Elemental reduction achievable with the HBA concept.

in the previous case, we control the azimuth direction ϕ by the direction of cavity wave travel. The electric fields in the cavity are

$$\begin{aligned} E_u &= -E_0 \cos \frac{\pi z}{h} e^{-\gamma u} \\ E_z &= \frac{\gamma h}{\pi} E_0 \sin \frac{\pi z}{h} e^{-\gamma u} = \frac{\gamma h}{\pi} E_0 \sin \frac{\pi z}{h} e^{-\gamma(x \cos \phi + y \sin \phi)} \end{aligned} \quad (5)$$

where the cavity occupies the region $-h/2 \leq z \leq h/2$, $\hat{\mathbf{u}} = \cos \phi \hat{\mathbf{x}} + \sin \phi \hat{\mathbf{y}}$ represents the travel direction, and $\gamma = \sqrt{(\pi/h)^2 - k_0^2}$ denotes the propagation constant. Note the odd symmetry of E_z along the z -dimension, we can also see that the TM1 mode is optimally excited when the phase of the top current strip π -phase-shifted from that of the bottom current strip. This aids our cause because this current distribution does not couple into the TEM fundamental mode and the two current strips can be fed by splitting a single feed, thus rendering the number of required feeds the same as for the TEM Huygens' box. The attractiveness of this design is that the metamaterial is no longer required within the cavity, hence simplifying the antenna and eliminating a source for loss and dispersion.

C. Elemental Reduction

We briefly discuss the HBA's merit in reducing the number of feed elements. To avoid grating lobes, elemental spacing in an array should not exceed $\lambda/2$ (for fair comparison, we consider a spacing of $\lambda/2$ for both the phased array and the HBA). For a square aperture of dimension $m\lambda \times m\lambda$, the number of elements required for the phased array is $N_{PA} = [m\lambda/(\lambda/2)]^2 = 4m^2$. On the other hand, the number of excitation elements required by the HBA is $N_{HBA} = 4 \times m\lambda/(\lambda/2) = 8m$. Consequently, an HBA achieves a reduction ratio of $m/2$. Fig. 5 depicts elemental reduction achievable using the HBAs as compared to a microstrip patch array of similar aperture dimensions. Clearly, the number of fed elements is dramatically reduced for large antenna apertures.

IV. SIMULATION RESULTS

We design and simulate the HBA models of Fig. 3(a) and (b) in ANSYS HFSS for radiation toward $(\phi, \theta) = (0^\circ, 45^\circ)$ from a Huygens' box size of $4\lambda \times 4\lambda$ at a frequency of 1 GHz. The TEM HBA has a height of $\lambda/6$ (set below $\lambda/2$ to avoid higher order modes), whereas the TM1 HBA has a height of $h = \lambda/\sqrt{2} = 212.0$ mm (as explained in Section III-B). We use an element spacing of $s = 0.5\lambda$ unless otherwise stated. For the TM1 HBA, the gap between the twin current strips is $g = \lambda/10$. The perforations on the top plates are subwavelength ($0.025\lambda \times 0.025\lambda$) with regular pattern and 0.125λ separation. As long as they are deeply subwavelength and evenly spaced, the

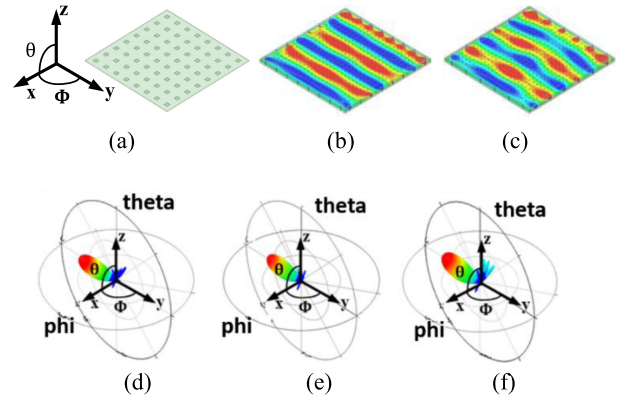


Fig. 6. (a) 8×8 microstrip patch array. (b) and (c) TEM HBAs with 32 sources and 24 sources, respectively, showing the generated waves. Radiation patterns of the (d) microstrip patch array, (e) TEM HBA with 32 sources, and (f) HBA with 24 sources.

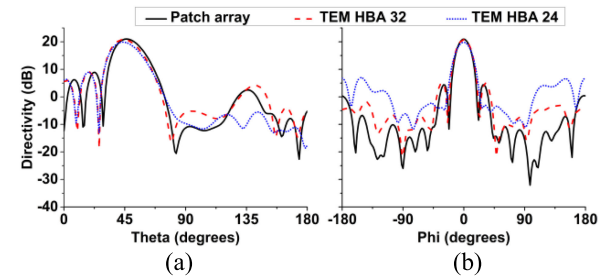


Fig. 7. TEM HBA radiation patterns at 1 GHz. (a) $\phi = 0^\circ$ plane. (b) $\theta = 45^\circ$ plane. Solid black lines represent the patch array, dashed red lines represent the TEM HBA with 32 sources, and dotted blue lines represent the TEM HBA with 24 sources.

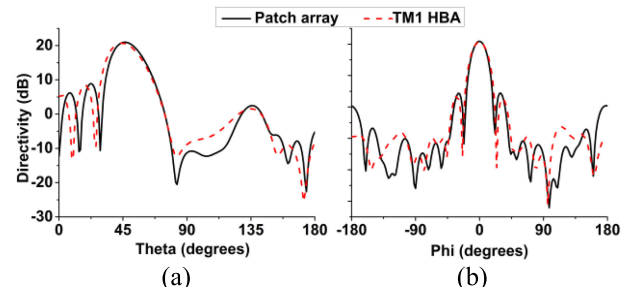


Fig. 8. Radiation patterns for the TM1 HBA. (a) $\phi = 0^\circ$ plane. (b) $\theta = 45^\circ$ plane. Solid black line represents the patch array, whereas dashed red line represents the TM1 HBA.

periodicity and arrangement of these perforations do not affect the radiation pattern. We calculate the TEM and TM1 fields in the HBA boxes using (3) and (5), respectively. Thereafter, we calculate the required complex excitation to synthesize these fields using (1) and (4).

To facilitate a comparison with the Huygens' box, we design a microstrip patch array of a corresponding aperture size on a Taconic RF-60 substrate ($\epsilon_r = 6.15$) backed by a ground plane. We present a diagram of the array in Fig. 6(a). The patch array is linearly phased to achieve radiation at $(\phi, \theta) = (0^\circ, 45^\circ)$ through the beam-steering relation $\alpha = -k_0 d \cos \theta$.

Fig. 6(a)–(c) shows the diagrams of the microstrip patch array, a TEM HBA, and a reduced-element TEM HBA; Fig. 6(d)–(f) shows their 3-D radiation patterns. Figs. 7 and 8 show the 2-D radiation patterns for the TEM and TM1 HBAs, respectively. In

TABLE I
SUMMARY OF RESULTS FOR 1 GHz $4\lambda \times 4\lambda$ APERTURE SIZE

	Patch Array(64 elements)	TEM HBA (32 Sources)	TEM HBA (24 Sources)	TM1 HBA
3dB BW (ϕ -dir.)	17.89°	20.03°	20.40°	20.28°
3dB BW (θ -dir.)	13.33°	19.40°	20.27°	19.66°
Main / First sidelobe level (ϕ – dir.)	16.7dB	16.8dB	17.2dB	17.3dB
Main / First sidelobe level (θ – dir.)	12.1dB	12.2dB	16.5dB	12.2dB

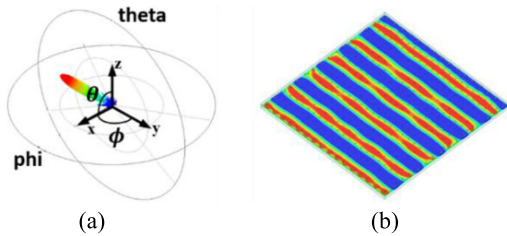


Fig. 9. (a) 3-D radiation plot for the 60 GHz TEM HBA. (b) Cavity wave (E_z) propagating at 0° with respect to the x -axis.

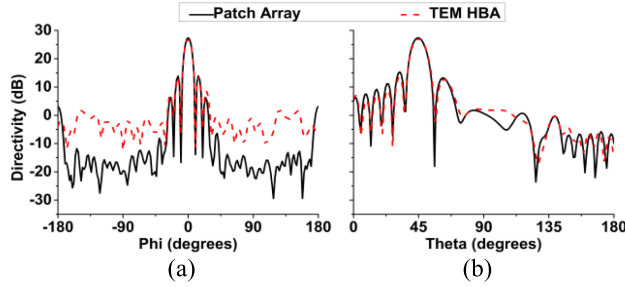


Fig. 10. Radiation patterns at 60 GHz: (a) $\theta = 45^\circ$ plane. (b) $\phi = 0^\circ$ plane. Solid black line represents the patch array, whereas dashed red line represents the TEM HBA.

all, we observe that the radiation patterns of the Huygens' boxes match very well to those obtainable from the microstrip patch array. We note that the wavelength within the TEM HBA is larger than the free-space wavelength: $\lambda_c = \lambda/n = \sqrt{2}\lambda$. We attempt to further reduce the number of fed elements by increasing the element spacing to 0.6λ . The resultant waveform is shown in Fig. 6(c). It is also in agreement with the microstrip patch array, but we observe some distortions in the cavity waves and some appreciable backside radiation. This is more clearly seen from the 2-D plot of the radiation patterns of Fig. 7. We present the key characteristics of the radiated beams in Table I.

As discussed in Section III-C and shown in Fig. 5, the HBA can achieve significant element reduction for large aperture antennas. We therefore design and simulate the TEM HBA of $8\lambda \times 8\lambda$ aperture at the mm-wave frequency of 60 GHz. Fig. 9 shows the simulated radiation beam and the corresponding cavity wave. Fig. 10 compares the radiation pattern from the HBA to a patch array of similar aperture size. Table II lists the key characteristics of the radiated beams. From these results, it can be seen that the HBA achieves a very similar radiation pattern to the patch array, but does with only 64 sources compared with 256 for the patch array, realizing a saving of 192 sources.

Finally, we show azimuthal beam steering for selected angles within $0^\circ \leq \phi < 90^\circ$ in Fig. 11. Equivalent results will be obtained for larger azimuthal angles due to the antenna's structural

TABLE II
SUMMARY OF RESULTS FOR 60 GHz $8\lambda \times 8\lambda$ APERTURE SIZE

	Patch Array(256 elements)	TEM HBA (64 Sources)
3dB Beamwidth (ϕ -dir.)	8.91°	8.62°
3dB Beamwidth (θ -dir.)	8.42°	8.78°
Main / First sidelobe level (ϕ)	11.75dB	11.40dB
Main / First sidelobe level (θ)	13.45dB	12.76dB

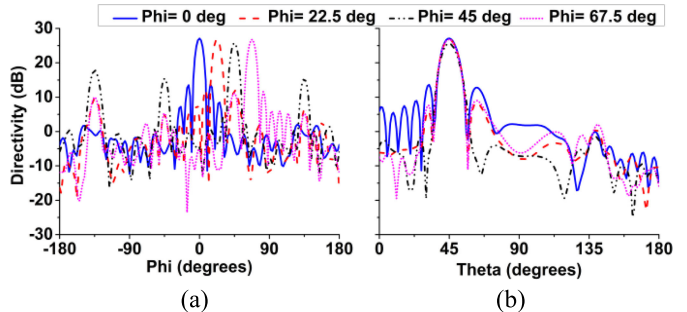


Fig. 11. TM1 HBA azimuthal beam steering at 60 GHz. Patterns are shown for wave propagation directions $\phi = 0^\circ, 22.5^\circ, 45^\circ, 67.5^\circ$ at (a) $\theta = 45^\circ$ plane and (b) $\phi = 0^\circ, 22.5^\circ, 45^\circ, 67.5^\circ$ planes.

symmetry. On the whole, we observe that the azimuthal angle is tuned according to the cavity wave's travel direction, whereas the elevation angle remains unchanged at 45° . We observe slightly stronger sidelobes and lower radiation peak strength as ϕ approaches 45° . This seems to be an artifact of imperfect plane wave generation in the Huygens' box. Nevertheless, beam steering is achieved while the beamwidth and sidelobe level remain largely stable.

We summarize the simulated results in Tables I and II.

V. CONCLUSION

In this letter, we have demonstrated two distinct models of a novel metasurface antenna that we call the HBA. These antennas produce highly directive radiation comparable to that of microstrip patch arrays of similar aperture sizes. We have shown that with the HBA, one can significantly reduce the number of radiating elements required and also achieve full beam steering. This reduction ratio becomes increasingly significant as the aperture size increases. Presented results depict radiation from antennas targeted at an angle $(\phi, \theta) = (0^\circ, 45^\circ)$. The simulated radiation patterns show good agreement with the patterns of a patch arrays of similar aperture sizes. Engineering the direction of cavity wave travel and the wavenumber allows one to steer the emitted radiation to any desired direction. The HBA shows great promise as a cost-effective alternative to phased arrays in high-gain antennas at mm-wave frequencies and beyond.

During the preparation of this letter, our attention was drawn to the work in [24] that excites peripheral sources around a cavity. As such, the device achieves reduction in the number of fed elements similar to our device. Our work differs from [24] in two important ways: First, by avoiding the use of a dense dielectric, we achieve a further reduction ratio than is shown in [24]. Second, by coupling from cavity to free space without momentum contribution from the perforation of the top plate, we achieve independent tuning in the azimuthal and elevation directions.

REFERENCES

- [1] R. J. Mailloux, *Phased Array Antenna Handbook*, 3rd ed. Norwood, MA, USA: Artech House, 2018.
- [2] A. H. Naqvi and S. Lim, "Review of recent phased arrays for millimeter-wave wireless communication," *Sensors*, vol. 18, no. 10, 2018, Art. no. 3194.
- [3] Y. Yusuf and X. Gong, "A low-cost patch antenna phased array with analog beam steering using mutual coupling and reactive loading," *IEEE Antennas Propag. Lett.*, vol. 7, pp. 81–84, 2008.
- [4] K. A. Oyesina and A. M. H. Wong, "The Huygens' box antenna: Metasurface-based directive antenna beam-steering with dramatically reduced elements," in *Proc. IEEE Int. Symp. Antennas Propag. USNC-URSI Radio Sci. Meeting*, Jul. 2019, pp. 443–444.
- [5] M. Chen, M. Kim, A. M. H. Wong, and G. V. Eleftheriades, "Huygens' metasurfaces from microwaves to optics: A review," *Nanophotonics*, vol. 7, pp. 1207–1231, 2018.
- [6] A. Epstein and G. V. Eleftheriades, "Huygens' metasurfaces via the equivalence principle: Design and applications," *J. Opt. Soc. Amer. B*, vol. 33, no. 2, pp. A-31–A-50, 2016.
- [7] A. Li, S. Singh, and D. Sievenpiper, "Metasurfaces and their applications," *Nanophotonics*, vol. 7, no. 6, pp. 989–1011, 2018.
- [8] C. L. Holloway, E. F. Kuester, J. A. Gordon, J. O. Hara, J. Booth, and D. R. Smith, "An overview of the theory and applications of metasurfaces: The two-dimensional equivalents of metamaterials," *IEEE Antennas Propag. Mag.*, vol. 54, no. 2, pp. 10–35, Apr. 2012.
- [9] W. Jan Krzysztofik and T. Nghia Cao, "Metamaterials in application to improve antenna parameters," in *Metamaterials and Metasurfaces*. London, U.K.: IntechOpen, 2019.
- [10] D. Binion, P. L. Werner, D. H. Werner, E. Lier, and T. H. Hand, "Metamaterial enhanced antenna systems: A review," in *Proc. Int. Appl. Comput. Electromagn. Soc. Symp.*, 2018, pp. 1–2.
- [11] R. W. Ziolkowski, "Metamaterial-based antennas: Research and developments," *IEICE Trans. Electron.*, vol. E89-C, pp. 1267–1275, 2006.
- [12] B.-I. Wu, W. Wang, J. Pacheco, X. Chen, T. M. Grzegorczyk, and J. A. Kong, "A study of using metamaterials as antenna substrate to enhance gain," *Prog. Electromagn. Res.*, vol. 51, pp. 295–328, 2006.
- [13] J. P. Turpin, Q. Wu, D. H. Werner, B. Martin, M. Bray, and E. Lier, "Low cost and broadband dual-polarization metamaterial lens for directivity enhancement," *IEEE Trans. Antennas Propag.*, vol. 60, no. 12, pp. 5717–5726, Dec. 2012.
- [14] E. Abdo-Sanchez, M. Chen, A. Epstein, and G. V. Eleftheriades, "A leaky-wave antenna with controlled radiation using a bianisotropic huygens' metasurface," *IEEE Trans. Antennas Propag.*, vol. 67, no. 1, pp. 108–120, Jan. 2019.
- [15] S. Lim, C. Caloz, and T. Itoh, "Metamaterial-based electronically controlled transmission-line structure as a novel leaky-wave antenna with tunable radiation angle and beamwidth," *IEEE Trans. Microw. Theory Techn.*, vol. 53, no. 1, pp. 161–173, Jan. 2005.
- [16] G. Minatti *et al.*, "Modulated metasurface antennas for space: Synthesis, analysis and realizations," *IEEE Trans. Antennas Propag.*, vol. 63, no. 4, pp. 1288–1300, Apr. 2015.
- [17] A. M. H. Wong and G. V. Eleftheriades, "A simple active Huygens source for studying waveform synthesis with Huygens metasurfaces and antenna arrays," in *Proc. IEEE Int. Symp. Antennas Propag. USNC/URSI Nat. Radio Sci. Meeting*, 2015, pp. 1092–1093.
- [18] A. M. H. Wong and G. V. Eleftheriades, "Active Huygens' metasurfaces for RF waveform synthesis in a cavity," in *Proc. 18th Mediterranean Electrotech. Conf.*, 2016, pp. 18–20.
- [19] A. M. H. Wong, "Active Huygens' box: Metasurface-enabled arbitrary electromagnetic wave generation inside a cavity," Oct. 2018, *arXiv:1810.05998*.
- [20] K. A. Oyesina, O. Z. Aly, G. G. L. Zhou, and A. M. H. Wong, "Active Huygens' box: Arbitrary synthesis of EM waves in metallic cavities," in *Proc. IEEE Appl. Comput. Electromagn. Soc. Symp.*, Miami, FL, USA, Apr. 2019, pp. 1–2.
- [21] A. M. H. Wong and G. V. Eleftheriades, "Experimental demonstration of the Huygens' box: Arbitrary waveform generation in a metallic cavity," in *Proc. IEEE Antennas Propag. Soc. Int. Symp. USNC/URSI Nat. Radio Sci. Meeting*, 2018, pp. 1893–1894.
- [22] T. J. Cui, D. R. Smith, and R. Liu, *Metamaterials: Theory, Design, and Applications*. Berlin, Germany: Springer, 2010.
- [23] S. Ramo, J. R. Whinnery, and T. Van Duzer, *Fields and Waves in Communication Electronics*. Hoboken, NJ, USA: Wiley, 1993.
- [24] A. H. Dorrah and G. V. Eleftheriades, "Peripherally excited phased arrays: Beam steering with reduced number of antenna elements," in *Proc. IEEE Can. Conf. Elect. Comput. Eng.*, Edmonton, AB, Canada, May 2019, pp. 1–4.